

We are IntechOpen, the world's leading publisher of Open Access books Built by scientists, for scientists

6,900

Open access books available

185,000

International authors and editors

200M

Downloads

Our authors are among the

154

Countries delivered to

TOP 1%

most cited scientists

12.2%

Contributors from top 500 universities



WEB OF SCIENCE™

Selection of our books indexed in the Book Citation Index
in Web of Science™ Core Collection (BKCI)

Interested in publishing with us?
Contact book.department@intechopen.com

Numbers displayed above are based on latest data collected.
For more information visit www.intechopen.com



Simplified Multi-Block Constitutive Model Predicting the Seismic Displacement of Saturated Sands along Slip Surfaces with Strain Softening

Constantine A. Stamatopoulos

Additional information is available at the end of the chapter

<http://dx.doi.org/10.5772/59657>

1. Introduction

Slopes consisting of saturated sands have recently moved down-slope tens or hundreds of meters under the action of earthquakes [1-3]. This large slide movement is usually associated with the generation of large excess pore pressures, as a result of grain crushing [3]. As these landslides have caused much destruction and fatalities, there is a need to propose easy-to-use and cost-effective methods predicting the triggering and movement of such slides.

The sliding-block model [4] is frequently used to simulate movement of slides triggered by earthquakes [5]. When ground displacement is large, this model may be inaccurate because of (a) reduction of shear resistance along the slip surface and (b) rotation of the sliding mass towards a more stable configuration [6]. It has been modeled in a cost-effective manner by an iterative procedure using the Jambu stability method by Deng et al [7], as well as by the multi-block model by Stamatopoulos et al. [8]. The multi-block model, described below, has the advantage of ensuring displacement compatibility during motion and will be applied in the present work.

Regarding effect (a) above, recently ring shear devices where sandy samples can be sheared under undrained conditions have been developed and applied to study the response of saturated sands along slip surfaces [2], [3], [9-15]. Constitutive equations modeling this soil response coupled with the multi-block sliding system model are needed in order to simulate the triggering of the slides and predict accurately the slide displacement. In the general case, constitutive models must be formulated in terms of effective stress in order to predict not only the shear stress, but also the generation of excess pore pressure along slip surfaces. Gerolymos and Gazetas [16] proposed an effective stress model predicting the displacement of saturated sands along slip surfaces based on grain crushing theory which requires 9 model parameters.

In addition, Stamatopoulos and Korai [17] proposed and validated with a number of ring shear tests a constitutive model in terms of effective stresses simulating the change of resistance along slip surfaces with shear displacement for sands either under undrained or drained conditions. The model requires 12 model parameters evaluation, which require the availability or performance of ring shear tests at different densities and drainage conditions.

On the other hand, in sliding-block models only the shear resistance versus shear displacement soil response affects the solution. This response depends on the drainage conditions and may alter as a result of dissipation of excess pore pressure in saturated sand. Yet, under earthquake-induced slides, triggering and slide movement are so rapid that dissipation of excess pore pressure does not occur and saturated sands behave in an undrained manner [1-3], [16]. It is inferred that for predicting the triggering and the slide movement of such slides, only the shear resistance versus shear displacement soil response under undrained conditions may be predicted.

The purpose of the present chapter is to present a cost-effective, but accurate, method predicting the triggering and displacement of slides consisting of saturated sands during earthquakes. For this purpose, first the shear stress -displacement response of saturated sands along slip surfaces is described and a model predicting this response with the minimum number of parameters is proposed, calibrated and validated. Then, this constitutive model is coupled with the multi-block sliding system model and the steps needed to predict earthquake-induced slide triggering and large displacement along slip surfaces of saturated sand using this improved model are specified in detail. Finally, the new improved method is validated by application at the well-documented Higashi Takezawa earthquake-induced slide.

2. Soil response

For the simulation of the response of sands along slip surfaces the ring shear device has the advantage that it is the only device where, similarly to landslides, shear displacement can be very large, larger than centimeters, or even meters. The sample in the ring-shear box is doughnut shaped. Undrained response is maintained by pressing a necessary contact pressure in order to keep the specimen volume constant. Additional details on the ring shear apparatus are given by Sassa et al. [18]. Ring-shear tests under both monotonic and cyclic loading have been performed and illustrated that the virgin shear stress-displacement response of saturated sands is almost identical under monotonic and cyclic loading [13]. This investigation also illustrated that the unloading-reloading stiffness is much larger than that due to virgin loading, especially when shear displacement that has already accumulated is considerable. Typical results are given in Fig. 1.

Table 1 gives tests found in the literature where saturated sands are sheared under undrained conditions in the ring shear device, the soils used in these tests, the initial density and stress conditions and the relevant references. Table 2 gives their particle diameter D_{50} and D_{10} . Fig 2 gives the measured shear stress-displacement response of these tests. In addition, table 1 and Fig. 3 gives two tests performed in a simple shear device that represent adequately the undrained response of the saturated sand along the slip surface of the Higashi Takezawa

landslide [1]. It can be observed that in all tests the shear stress first increases at a decreasing rate with shear displacement and reaches its peak value in a few millimeters or centimeters. Then, it decreases at a decreasing with shear displacement rate and reaches its residual value in many centimeters or meters.

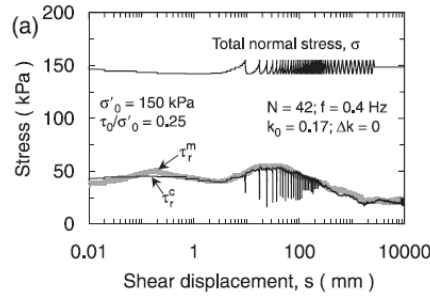


Figure 1. Typical measured effect of cyclic loading on shear stress-displacement relationship. (Trandafir and Sassa [13]).

| Test no | Ref. | Sand name | Dr% | σ'_0 (kPa) | τ_0 (kPa) |
|---------|------|-----------|-----|-------------------|----------------|
| 1 | [9] | S8 | 62 | 196 | 56 |
| 2 | [9] | S8 | 63 | 196 | 0 |
| 3 | [9] | S8 | 63 | 196 | 4 |
| 4 | [10] | S8 | 63 | 200 | 0 |
| 5 | [9] | S8 | 65 | 196 | 56 |
| 6 | [9] | S8 | 68 | 196 | 56 |
| 7 | [9] | S8 | 68 | 196 | 0 |
| 8 | [9] | S8 | 69 | 196 | 40 |
| 9 | [9] | S8 | 69 | 196 | 75 |
| 10 | [9] | S8 | 69 | 196 | 110 |
| 11 | [9] | S8 | 95 | 196 | 0 |
| 12 | [11] | ING | 29 | 202 | 0 |
| 13 | [11] | ING | 29 | 262 | 0 |
| 14 | [11] | ING | 32 | 290 | 0 |
| 15 | [12] | ING | 44 | 196 | 0 |
| 16 | [12] | ING | 44 | 280 | 9 |
| 17 | [12] | ING | 44 | 374 | 9 |
| 18 | [11] | WG | 30 | 196 | 0 |
| 19 | [11] | WG | 30 | 250 | 0 |
| 20 | [11] | WG | 30 | 290 | 0 |
| 21 | [12] | WG | 44 | 203 | 0 |
| 22 | [12] | WG | 44 | 235 | 0 |
| 23 | [12] | WG | 44 | 290 | 0 |
| 24 | [12] | WG | 44 | 366 | 0 |
| 25 | [1] | Higashi | | 50 | 35 |
| 26 | [1] | Higashi | | 99 | 40 |

Table 1. Constant-volume ring shear tests in saturated sands found in the literature. Relevant reference (Ref.), sand name and initial conditions are given.

| | WG | ING | S8 |
|----------|------|------|-------|
| D50 (mm) | 0.23 | 0.11 | 0.06 |
| D10 (mm) | 0.04 | 0.03 | 0.015 |

Table 2. D50 and D10 values of the sands reported in table 1.

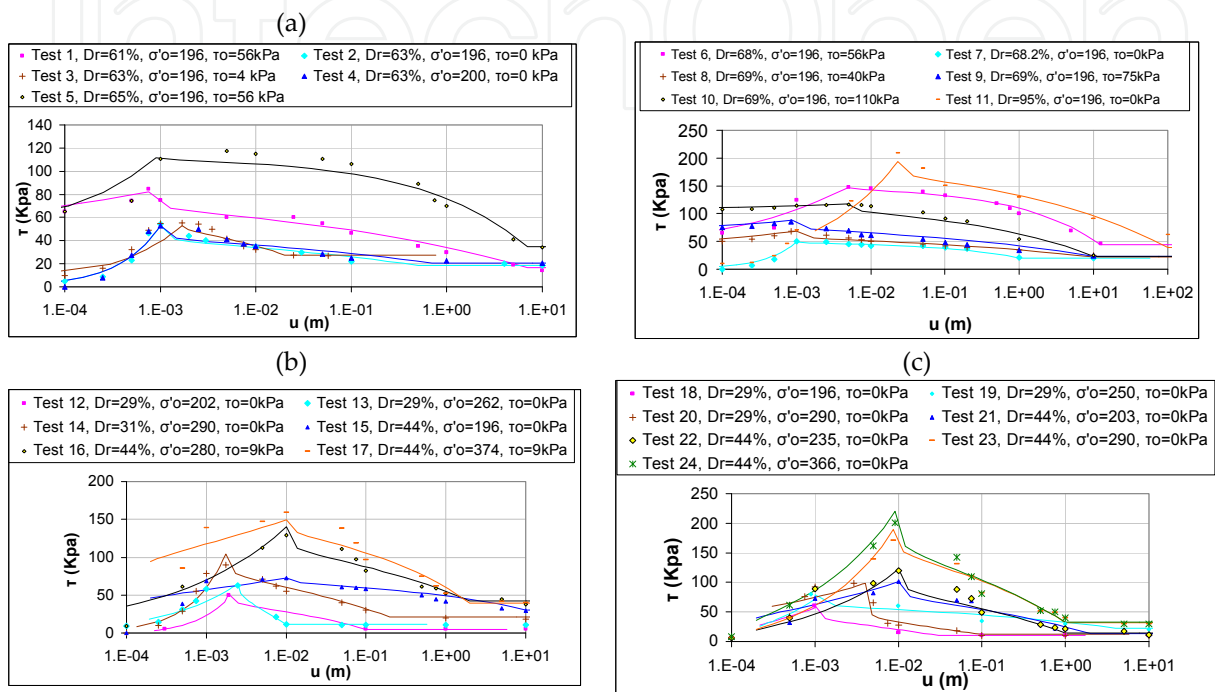


Figure 2. Shear stress-displacement response of the constant-volume ring shear tests of table 1. Tests on sands (a) S8, (b) ING, (c) WG. Model predictions are also given.

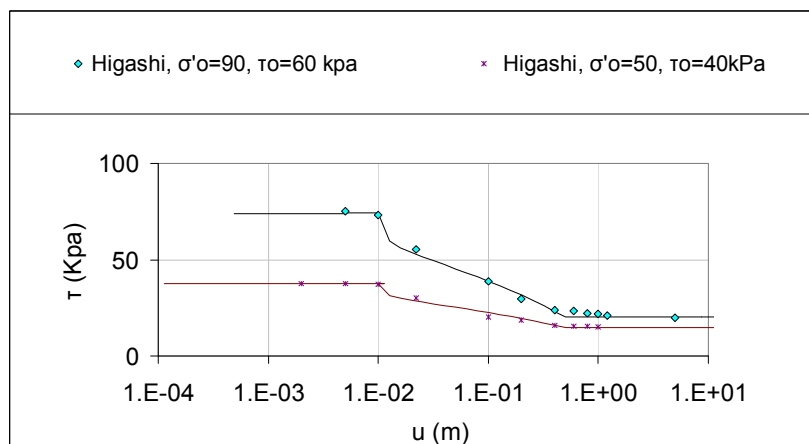


Figure 3. Shear stress-displacement response of the constant-volume ring shear tests of table 1. Tests on the Higashi Takezawa landslide. Model predictions are also given.

3. Proposed model

The following simplified equations are used to simulate shear stress-displacement response of sands under undrained conditions:

$$\begin{aligned}
 \tau &= \sigma'_0 R \text{ where} & (a) \\
 \text{For } 0 < u < u_1 & R = R_{res} \frac{u^{a_1}}{r u_1^{a_1}} & (b) \\
 \text{For } u_1 > u > u_2 & R_{res} \left\{ \frac{1}{r} - \left(\frac{1}{r} - 1 \right) \frac{(u - u_1)^{a_2}}{(u_2 - u_1)^{a_2}} \right\} & (c) \\
 \text{For } u > u_2 & R = R_{res} & (d)
 \end{aligned} \tag{1}$$

where σ'_0 is the applied effective normal stress and u is the shear displacement. The model has 6 parameters: R_{res} , r , u_1 , u_2 , a_1 , a_2 . As illustrated in Fig. 4, R_{res} is the stress ratio (τ/σ'_0) of the material at the residual state. The parameter r equals to (R_{res}/R_{max}). Thus, it varies from 0 to 1. The parameters (a) u_1 and (b) u_2 give the shear displacement corresponding to (a) the peak shear stress and (b) the minimum shear displacement corresponding to the residual shear stress. The parameters (i) a_1 and (ii) a_2 determine the rate of change of the shear stress with shear displacement for (i) $u_1 < u$ and (ii) $u_1 < u < u_2$ respectively.

In the proposed constitutive model plastic shear displacements are assumed to accumulate when the stress ratio (τ/σ') increases, while the elastic shear displacement is ignored. This is consistent with the response depicted in Fig. 1.

An excel worksheet was programmed to simulate the undrained response of sands, as described by equations (1). A modification is needed for tests with initial shear stress (τ_0). In this case the shear displacement is u' and equals:

$$u' = u - u_0 = u - u_1 \left[\frac{\tau_0}{\sigma'_0 R_m} \right]^{\frac{1}{a_1}} \quad u' > 0 \tag{2}$$

where u is the displacement predicted by eq. (1).

The model parameters of the tests of Table 1 were estimated using the procedure described above. They are given in Table 3. In addition, Fig. 2 gives the computed shear stress-displacement curves. Table 3 gives the standard deviation of the ratio of predicted by measured values of all points defining the shear stress-displacement curves of all tests. It can be observed that in all tests the standard deviation is less than 0.3, while the average value is 0.12. In addition, from Fig 2 it can be observed that adequate prediction of undrained response is achieved in all tests. Furthermore, from table 3 it can be observed that the values of the model parameters used do not vary considerably from case to case and are in general in a rational range: the parameters a_1 and a_2 do not take values greater than 1 and less than 0 and the parameter R_m generally increases with D_r . All the above verify the proposed model.

Advantage of the proposed model is simplicity. However, it has the disadvantage of generality. Inspection of table 3, illustrates that the model parameters depend on the relative density, confining stress and initial shear stress. Thus, when applying this simplified model, tests with similar relative density, confining stress and initial shear stress as that existing in-situ should be used.

| Test no | Rm | r | u1 (m) | u2 (m) | a1 | a2 | N | SDev (Pred/Meas) |
|----------|------|------|--------|--------|------|------|----|------------------|
| 1 | 0.42 | 0.20 | 0.001 | 7.00 | 0.08 | 0.16 | 12 | 0.07 |
| 2 | 0.27 | 0.35 | 0.001 | 0.50 | 1.00 | 0.15 | 11 | 0.17 |
| 3 | 0.27 | 0.52 | 0.002 | 0.02 | 0.57 | 0.48 | 12 | 0.15 |
| 4 | 0.27 | 0.39 | 0.001 | 0.70 | 1.00 | 0.15 | 10 | 0.12 |
| 5 | 0.57 | 0.31 | 0.001 | 7.00 | 0.30 | 0.40 | 12 | 0.18 |
| 6 | 0.75 | 0.30 | 0.005 | 12.50 | 0.20 | 0.40 | 12 | 0.13 |
| 7 | 0.25 | 0.42 | 0.001 | 1.00 | 1.00 | 0.38 | 10 | 0.12 |
| 8 | 0.35 | 0.32 | 0.001 | 10.00 | 0.10 | 0.14 | 12 | 0.07 |
| 9 | 0.45 | 0.26 | 0.001 | 10.00 | 0.08 | 0.15 | 12 | 0.10 |
| 10 | 0.60 | 0.20 | 0.005 | 10.00 | 0.02 | 0.24 | 12 | 0.07 |
| 11 | 0.99 | 0.20 | 0.023 | 100.00 | 0.40 | 0.20 | 9 | 0.15 |
| 12 | 0.24 | 0.10 | 0.002 | 0.10 | 1.00 | 0.30 | 5 | 0.01 |
| 13 | 0.25 | 0.17 | 0.003 | 0.01 | 0.50 | 0.40 | 11 | 0.17 |
| 14 | 0.36 | 0.23 | 0.002 | 0.50 | 1.00 | 0.15 | 10 | 0.12 |
| 15 | 0.37 | 0.42 | 0.010 | 10.00 | 0.10 | 0.25 | 1 | 0.14 |
| 16 | 0.50 | 0.30 | 0.010 | 2.00 | 0.30 | 0.20 | 10 | 0.18 |
| 17 | 0.40 | 0.26 | 0.010 | 2.00 | 0.10 | 0.30 | 11 | 0.14 |
| 18 | 0.30 | 0.17 | 0.001 | 0.03 | 0.35 | 0.20 | 6 | 0.14 |
| 19 | 0.30 | 0.30 | 0.001 | 4.00 | 0.50 | 0.15 | 4 | 0.16 |
| 20 | 0.34 | 0.12 | 0.004 | 0.10 | 0.20 | 0.10 | 9 | 0.18 |
| 21 | 0.50 | 0.13 | 0.010 | 2.00 | 0.20 | 0.20 | 10 | 0.18 |
| 22 | 0.52 | 0.12 | 0.010 | 1.00 | 0.40 | 0.20 | 11 | 0.17 |
| 23 | 0.65 | 0.17 | 0.009 | 1.00 | 0.50 | 0.25 | 10 | 0.14 |
| 24 | 0.60 | 0.15 | 0.009 | 1.00 | 0.40 | 0.20 | 9 | 0.15 |
| 25 | 1.10 | 0.28 | 0.020 | 10.00 | 0.40 | 0.25 | 5 | 0.05 |
| 26 | 0.60 | 0.28 | 0.010 | 5.00 | 0.05 | 0.20 | 6 | 0.04 |
| All Mean | | | | | | | | 0.12 |
| All SDev | | | | | | | | 0.05 |

Table 3. The parameters of equation (1) that fit the tests of table 1. Statistical analysis of the accuracy of the predictions is also given, where N represents the number of points defining the shear stress-displacement curve of each test.

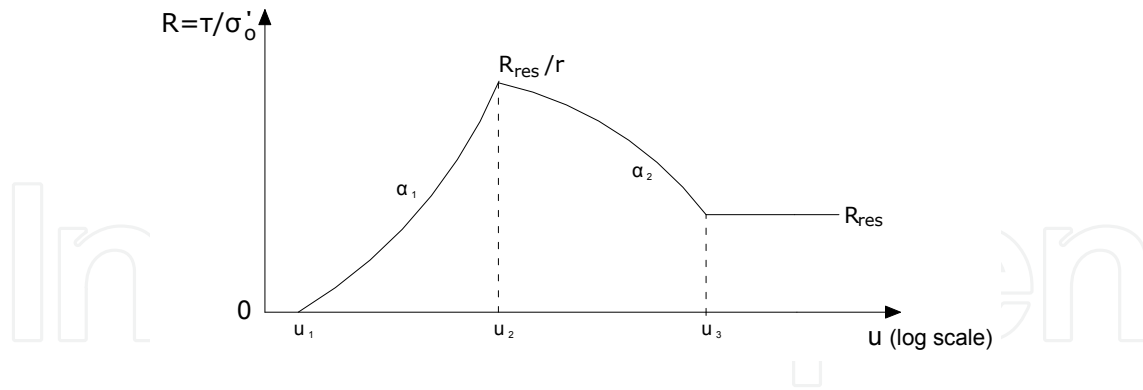


Figure 4. The proposed model and its model parameters.

4. The Multi-Block Sliding System Model

4.1. Introduction

A slip surface which consists of linear segments is considered (Fig. 5a). In order for the mass above the slip surface to move, interfaces inside the sliding mass must be formed at the nodes between the linear segments [20]. In this manner the mass is divided into n blocks. Soil is assumed to behave as a rigid-perfectly plastic material with a Mohr-Coulomb failure criterion at both the slip surface and the interfaces. The forces that are exerted in block “ i ” are given in Fig. 5a.

When the slide moves, two options exist regarding the relative movement of blocks: (a) no separation and (b) separation. When blocks are not separated, the velocity must be continuous at the interface. This rule predicts that the relative displacement of the n blocks is related to each other as:

$$\frac{du_i}{du_{i+1}} = \frac{\cos(\delta_i + \beta_{i+1})}{\cos(\delta_i + \beta_i)} \quad (3)$$

where u is the displacement moved by the sliding mass along the linear segment “ i ” of the trajectory, d refers to increment, the subscripts i and $i+1$ refer to trajectory segments i and $i+1$ counting uphill and β_i and $(90-\delta_i)$ are the inclinations of the trajectory segment and interface i respectively.

Fig. 5a illustrates the forces exerted in each block i . In the case that separation of blocks does not occur and a horizontal acceleration is applied, as indicated by Stamatopoulos et al [8], the governing equation of motion is

$$\ddot{u}(t) \cdot \sum_{i=1}^n \left(m_i q_i \cos(\phi_i) \cdot \prod_{j=i}^{n-1} \frac{dd_{j+1}}{ff_j} \right) = \sum_{i=1}^{n-1} \left([-bc_i \cos(\phi b_i) + Ub_i \sin(\phi b_i)] \cdot \frac{ss_i}{ff_i} \cdot \prod_{j=i}^{n-1} \frac{dd_{j+1}}{ff_j} \right) + \sum_{i=1}^n \left(\{xx_i (m_i g k(t) + H_i) - v_i [m_i g + Q_i] - c_i l_i \cos(\phi_i) + U_i \sin(\phi_i)\} \cdot \prod_{j=i}^{n-1} \frac{dd_{j+1}}{ff_j} \right) \tag{a}$$

where

$$ss_i = \sin(\beta_{i+1} - \beta_i + \varphi_i + \phi b_{i+1}) \tag{b}$$

$$ff_i = \cos(\varphi_i + \phi b_{i+1} - \beta_i - \delta_i) \tag{c}$$

$$xx_i = \cos(\varphi_i - \beta) \tag{c}$$

$$v_i = \sin(\varphi_i - \beta_i) \tag{d}$$

$$dd_i = \cos(\varphi_i + \phi b_i - \beta_i - \delta_{i-1}) \tag{e}$$

$$q_i = \prod_{j=i}^{n-1} \frac{\delta \cos(\beta_{j+1} + \beta_j)}{\delta \cos(\beta_j + \beta_{j+1})} \tag{f}$$

where u is the relative shear displacement of the uppermost block (block n), down-hill displacements being considered positive, g is the acceleration of gravity, Q_i is the vertical external load on block i , H_i is the horizontal external load on block i , m_i is the mass of block i , U_i is the pore water force acting on block i and Ub_i is the pore water force along the interface between blocks i and $i+1$, φ_i and c_i is the angle of friction and cohesion on the slip surface at block i along the slip surface and ϕb_i and cb_i is the angle of friction and cohesion on the interslice surface between blocks i and $i+1$. It should be noted that all the above masses and forces are taken per unit length, normal to the paper in Fig. 5a.

Equation (4) can be written in the form

$$\ddot{u}_i = Z_i g (k(t) - k_c) \text{ where} \tag{a}$$

$$Z_i = \frac{\sum_{i=1}^n \left(-xx_i m_i \cdot \prod_{j=i}^{n-1} \frac{dd_{j+1}}{ff_j} \right)}{\sum_{i=1}^n \left(m_i q_i \cos(\phi_i) \cdot \prod_{j=i}^{n-1} \frac{dd_{j+1}}{ff_j} \right)} \tag{b}$$

$$k_c = \frac{\sum_{i=1}^{n-1} \left([cb_i b_i \cos(\phi b_i) - Ub_i \sin(\phi b_i)] \cdot \frac{ss_i}{ff_i} \cdot \prod_{j=i+1}^{n-1} \frac{dd_{j+1}}{ff_j} \right) + g \cdot \sum_{i=1}^n \left(-xx_i m_i \cdot \prod_{j=i}^{n-1} \frac{dd_{j+1}}{ff_j} \right)}{\tag{5}}$$

$$+ \frac{\sum_{i=1}^n \left(\{-xx_i (H_i) + v_i [W + Q_i] + c_i l_i \cos(\phi_i) - U_i \sin(\phi_i)\} \cdot \prod_{j=i}^{n-1} \frac{dd_{j+1}}{ff_j} \right)}{g \cdot \sum_{i=1}^n \left(-xx_i m_i \cdot \prod_{j=i}^{n-1} \frac{dd_{j+1}}{ff_j} \right)} \tag{c}$$

where k_c is the critical acceleration factor, defined as the limit horizontal acceleration needed to initiate motion (a_c) normalized by the acceleration of gravity (g).

For large displacement, the masses and lengths of each block in equation (5) must be updated in terms of the distance moved. Assuming that the displacement u is less than the initial length of l_n , the change of lengths l_i in each displacement increment Δu equals

$$\begin{aligned} \Delta l_i &= \Delta u \cdot q_i & (a) \\ \Delta l_n &= -\Delta u & (b) \\ \Delta l_2 &= \Delta l_3 = \dots = \Delta l_{n-1} = 0 & (c) \end{aligned} \quad (6)$$

The incremental change in the interslice lengths b_i is

$$\Delta b_i = \frac{\sin \theta_i}{\cos(\theta_i + \beta_i + \delta_i)} \cdot q_i \Delta u \quad (7)$$

where the angle θ_i is given in Fig. 5b. Fig. 5c illustrates the deformation that these rules predict. In addition, the incremental change in the mass is

$$\begin{aligned} \Delta m_i &= \rho_{i+1} \{ b_{(i+1)-c} \cdot \cos(\beta_{i+1} + \delta_{i+1}) \cdot q_i \Delta u + \frac{0.5 \cdot \cos(\beta_{i+1} + \delta_{i+1}) \cdot \sin \theta_{i+1}}{\cos(\theta_{i+1} + \beta_{i+1} + \delta_{i+1})} \cdot (q_i \Delta u)^2 \\ &- b_{i-c} \cdot \cos(\beta_i + \delta_i) \cdot q_i \Delta u - \frac{0.5 \cdot \cos(\beta_i + \delta_i) \cdot \sin \theta_i}{\cos(\theta_i + \beta_i + \delta_i)} \cdot (q_i \Delta u)^2 \} \end{aligned} \quad (8)$$

where b_{i-c} and $b_{(i+1)-c}$ correspond to the values of b_i and $b_{(i+1)}$ at the previous increment and q is the total unit weight of the soil.

Separation of blocks occurs when an interslice force, N_i , is negative [21]. Fig. 6c illustrates a typical case where this occurs: when the angle β_m at the trajectory is larger than the angle β_{m+1} . In this case, the soil mass of the block along the "m+1" segment of the trajectory cannot maintain contact with the rest of the sliding material and is detached from the system. The detached mass is no longer considered in the solution.

4.2. Multi-block model with constitutive equations

The multi-block sliding system can be coupled with the constitutive model described above by assuming zero cohesion and varying only the friction angles, φ_i , of equation (5) as

$$\varphi_i = \arctan \left(\frac{\tau_i}{\sigma'_{o-i}} \right) \quad (9)$$

In equation (9), τ_i and σ'_{o-i} are the shear stress and the initial (prior to slide movement) effective normal stress at the base of block i .

Application of eq. (9) with the multi-block numerical code first requires to estimate the shear initial stresses τ_i , or equivalently, the initial friction angles φ_i . This is performed by iterations, by assuming all φ_i are equal and by increasing them incrementally until critical equilibrium is

achieved in the initial slide configuration. Then, at each increment, for each block, τ_i is updated from equations (1) in terms of the incremental shear displacement. It should be noted that the values of τ , u and σ'_o of equations (1) correspond to τ_i , u_i and σ'_{o-i} in equation (9).

4.3. Computer program

A computer program which solves the equations described above has been developed by the author. The input geometry is specified as the nodes of the linear segments defining the trajectory, ground and water table surfaces. Different soil properties may be specified at each segment of the slip surface and at the interfaces. Along the slip surface the Mohr-Coulomb Model or the constitutive model may be applied. At the interfaces the Mohr-Coulomb Model is applied. Output of the program includes the final slide geometry and acceleration velocity and displacement of nodes of the sliding mass versus time.

Pore pressures at the mid-points of the linear segments of the slip and the interfaces prior to the application of earthquake loading are estimated from the water table surface according to the general equation:

$$P_i = h_{w-i} \cos^2(\theta w_i) \quad (10)$$

where θw_i is the inclination and h_i is the height of the water table surface above the mid-point of slip segment "i". The program includes graphical representations of the input and final geometries of the slope. More details of the multi-block method and the associated numerical code are given by Stamatopoulos et al [8].

4.4. Application of the model along (pre-defined) slip surfaces and very large displacement under earthquake loading

In the case that the slip surface is not pre-existing, generally, application of the sliding-block model first requires the prediction of the location of the slip surface by stability analysis. However, this determination, and the ability of stability methods to estimate the location of this slip surface is beyond the purpose of the present work.

In order to apply the improved multi-block model along pre-defined slip surfaces under earthquake loading first the slip surface, ground surface and water table surface are simulated as a series of linear segments. If the inclinations of the interfaces is not predefined according to existing faults, as proposed by Sarma [20] they are obtained based on the condition of the minimum critical acceleration value, by iterations. Along the slip surface the Mohr-Coulomb model the value is used with soil strength corresponding to large displacement, as it is the most representative of the soil strength during occurrence of the landslide. At the interfaces, peak values of strength are used. The reason is that as the internal interfaces are fixed in space, they are continuously reforming with new material and thus the strength cannot be at residual [23]. In addition, at large deformations the method described above to estimate the interslice angles of the sliding mass according to the condition of minimum critical acceleration at the initial slide configuration may not be adequate. The reason is that some segments of the trajectory do not have mass at the initial configuration and thus their interface angles cannot

be defined. This can be resolved by applying the criterion of minimum acceleration not only at the initial, but also at the final slide configuration and taking the average values at the common interfaces of the two interfaces. The final slide configuration can be obtained by applying the multi-block model assuming that the interface angles not defined at the initial slide configuration equal zero.

The slide triggering is investigated and the potential slide deformation is estimated using the multi-block model. For the representative seismic motion, the proposed constitutive model is used along the slip surface, while at the interfaces the Mohr-Coulomb model with peak values of strength is used.

5. Application at the Higashi Takezawa landslide

5.1. The slide

Fig. 6 gives the cross-section of the Higashi Takezawa landslide [1]. According to Deng et al. [1] a representative acceleration record for the slide is that reported by the Japan Meteorological Agency (JMA) in 2004. It is given in Fig. 6. Triaxial and shear laboratory tests of material along the slip surface of the slide have been performed by Deng et al., [1] and are given in Fig. 6.

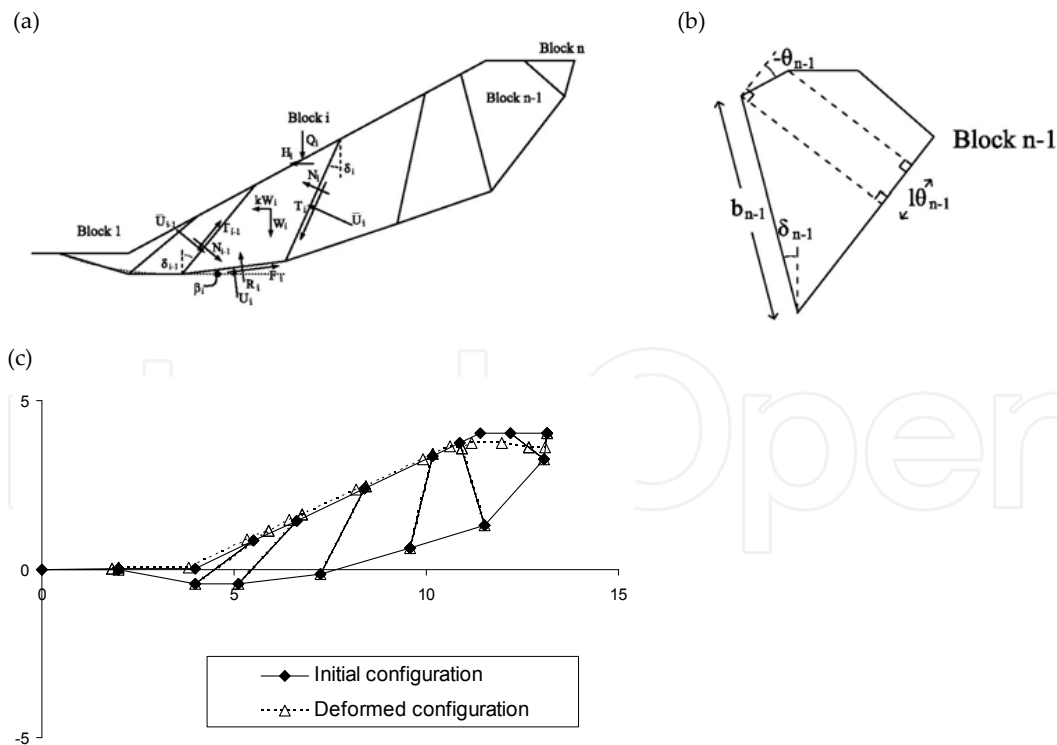


Figure 5. (a) The multi-block stability method proposed by Sarma (1979). (b) Definition of the angle θ_i of the ground surface of block i. The angle θ_i changes when $u_i > u_{\theta_i}$ (c) Deformation assumed in the multi-block model for a case of two blocks. The x-axis gives the horizontal distance, while the y-axis gives the elevation.

5.2. Model predictions

First the model parameters of the constitutive model are obtained by the prediction of the shear test results. Table 4 gives the model parameters and Fig. 7 compares model predictions of the constitutive model with the measured response. Very good agreement is observed. It can be observed that even though all model parameters do not depend on the applied normal stress, predictions are adequate.

From Fig. 6 it can be observed that all of the slip surface is below the water table line. In addition, according to Deng et al. [1] the material at the slip surface is approximately uniform. Thus, the model parameters of Table 4 are used to simulate the soil response at the slip surface. At the interfaces, the peak soil strength must be used, which, according to the results of the triaxial tests, equals $\varphi'=36^\circ$.

Typically, the criterion of minimum critical acceleration factor at the initial and final configurations is applied to estimate the interface angles of the sliding mass. The Mohr Coulomb model was applied both along the slip surface and at the interfaces. Along the slip surface the residual soil strength was applied, while at the interface the peak soil strength. Fig. 8 gives the critical acceleration in terms of the interslice angles at the (a) initial and (b) final slide configurations. Table 5 gives the obtained interslice angles according to the criterion of minimum acceleration factor and the results of Fig. 8.

Once the interface angles are obtained, the multi-block model with the constitutive model along the slip surface is applied. Fig. 9a gives the input geometry used to simulate the slide with the multi-block model. As the seismic motion of Fig. 6d is applied, Fig. 10 gives the computed equivalent friction angle of block 2 (equation (9) and the slide acceleration (a), velocity (V) and distance moved (u). In addition, Fig. 9b gives the computed versus measured final slide configuration. It can be observed that the proposed method predicted both the triggering of the slide and with good accuracy the final slide configuration. From Fig. 9 it can be observed, as the earthquake is applied, some shear displacement accumulates. This causes the friction angle at the base of the blocks to increase. Once the peak friction angle is reached, due to material softening, the friction angle decreases, to its residual value. At this point, the critical acceleration of the sliding system is negative (this means that the slide is unstable) and the slide velocity starts to increase and displacement to accumulate rapidly. As the slide moves, the mass slides at a progressively smaller average inclination. The critical acceleration of the sliding mass gradually increases and it becomes positive. Then, the slide velocity starts to decrease, and becomes zero at $t=51s$.

Finally, parametric analyses were performed. In some of these the Mohr-Coulomb with residual or maximum strength was applied, while in other no seismic motion was applied. Their results are given in Table 6. They illustrate that even though for the prediction of the triggering of the slide the applied motion and the constitutive model are important, for the prediction of the final slide configuration, use of the Mohr-coulomb model with the residual soil strength produces relatively accurate results, even when the seismic motion is not applied.

| Rm | r | u1 (m) | u2 (m) | a1 | a2 |
|-----|-----|--------|--------|-----|------|
| 0.8 | 0.3 | 0.01 | 0.5 | 0.3 | 0.25 |

Table 4. The Higashi Takezawa landslide. Model parameters

| i= | Initial config. | Final config. | Mean value |
|----|-----------------|---------------|------------|
| 1 | - | 30° | 30° |
| 2 | -20° | 10° | -5° |
| 3 | -10° | - | -10° |

Table 5. The Higashi Takezawa landslide. Obtained interslice angles (δ_i) according to the criterion of minimum acceleration and the result of Fig. 8.

| Seismic Motion | Soil model | u (m) |
|----------------|-------------------------------------|-------|
| Yes | Constitutive | 376 |
| Yes | Mohr-Coulomb with residual strength | 414 |
| Yes | Mohr-Coulomb with maximum strength | 0.25 |
| No | Mohr-Coulomb with residual strength | 427 |
| No | Mohr-Coulomb with maximum strength | 0 |

Table 6. Parametric analyses. Slide displacement in terms of the soil model and seismic motion applied.

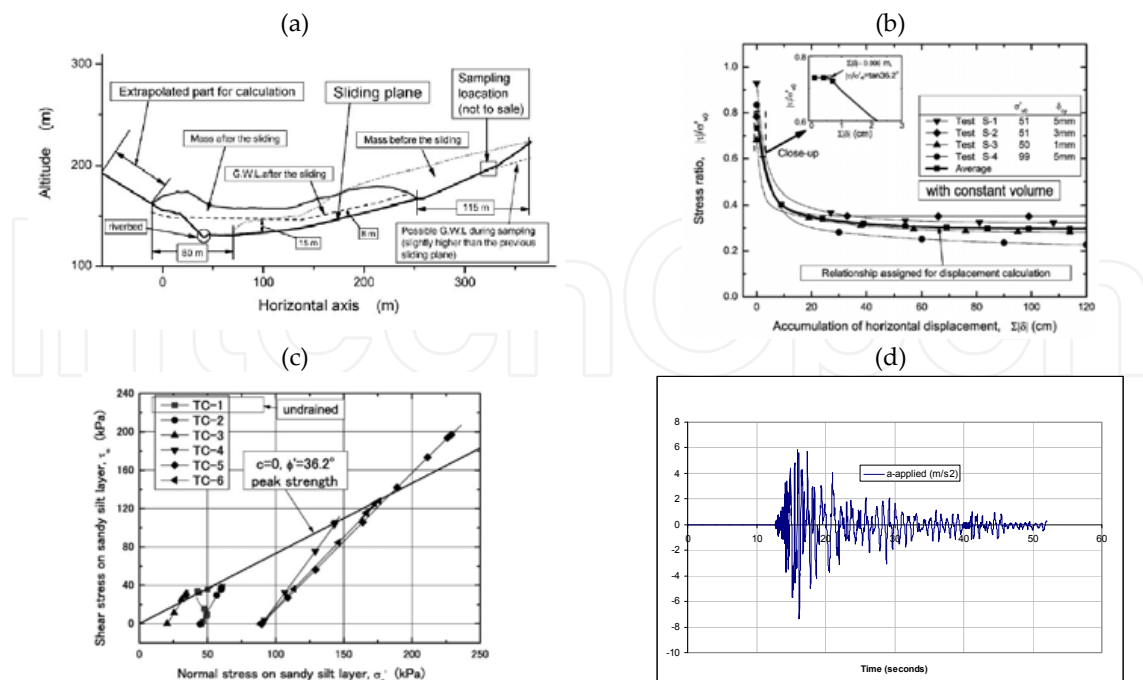


Figure 6. The Higashi Takezawa landslide. (a).Cross-section of slide (Deng et al. [1]), (b). Simple shear test results (Deng et al. [1]), (c) Triaxial test results (Deng et al. [1]), (d) representative applied acceleration in terms of time (Deng et al. [1])

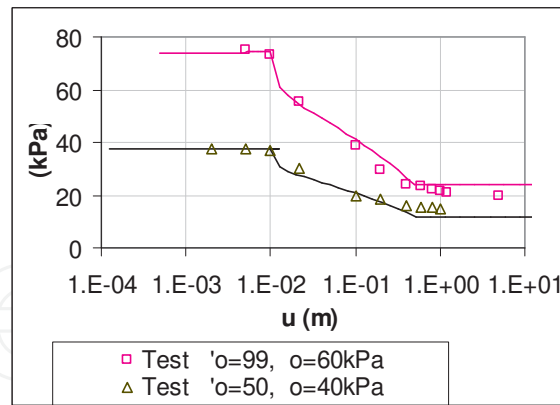


Figure 7. The Higashi Takezawa landslide. Computed versus measured response in terms of initial consolidation stress for the unique model parameters of table 4.

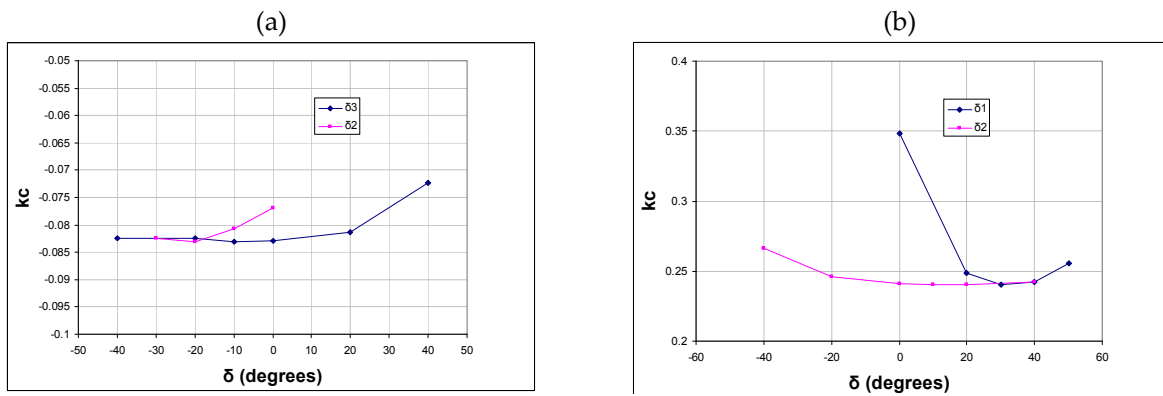


Figure 8. The Higashi Takezawa landslide. Critical acceleration in terms of the interslice angles. (a) Initial slide configuration, (b) Final slide configuration.

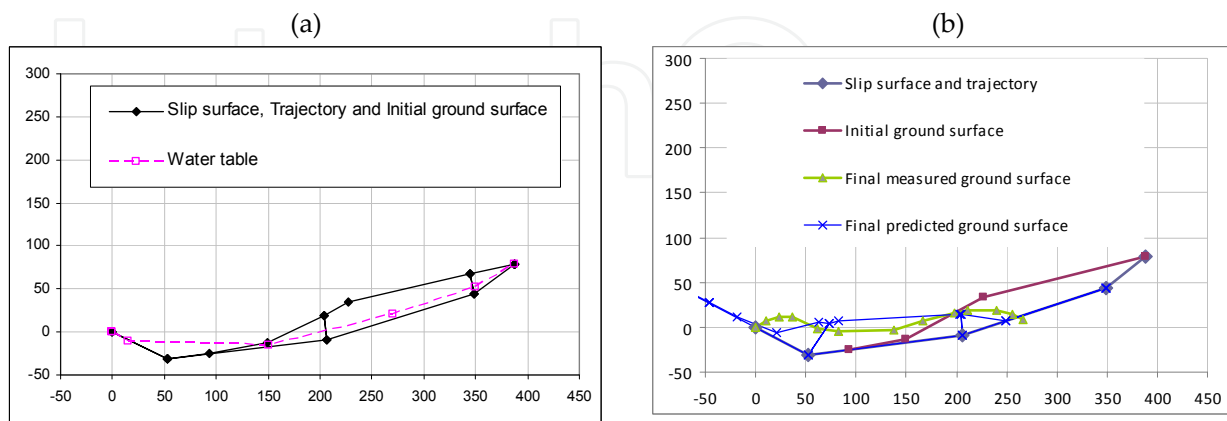


Figure 9. The Higashi Takezawa landslide. (a). Input used to simulate the slide with the multi-block model, (b). Computed versus measured final slide configuration.

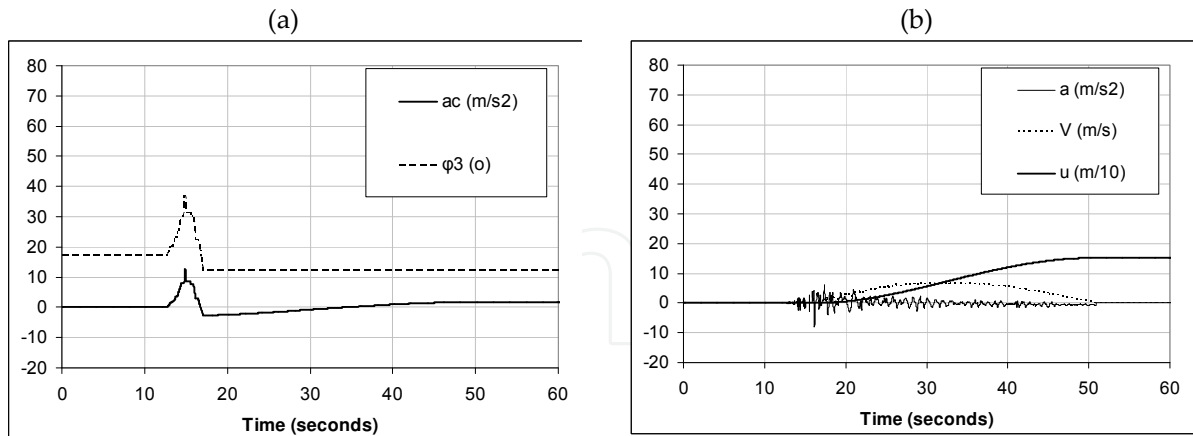


Figure 10. (a). Computed equivalent friction angle of block 3 and critical acceleration of the slide (a_c) and (b) slide acceleration (a), velocity (v), distance moved (u), all in terms of time

6. Conclusions

Slopes consisting of saturated sands have moved down-slope tens or hundreds of meters under the action of earthquakes recently. The chapter presents a simplified method predicting the triggering and displacement of such earthquake-induced slides of saturated sands.

For this purpose, a simplified constitutive model simulating soil response of saturated sands along slip surfaces is proposed. Comparison of the model predictions with results of ring shear tests illustrated that the model predicts with good accuracy the shear stress-displacement response of saturated sands. Advantage of the proposed model is simplicity. However, it has the disadvantage of generality. Thus, when applying this simplified model, tests with similar relative density, confining stress and initial shear stress as that existing in-situ should be used.

Then, this constitutive model was coupled with the multi-block sliding system model to predict the triggering and displacement of earthquake-induced slides of saturated sands. The multi-block model considers a general mass sliding on a slip surface which consists of n linear segments. In order for the mass to move, at the nodes between the linear segments, interfaces inside the sliding mass must be formed. Steps needed to apply the method are: (a) define the trajectory, ground and water table surfaces, (b) obtain the model parameters of the soil resistance by the results shear tests, (c) obtain the interface angles by applying the principle of minimum critical acceleration factor and (d) to simulate the triggering and displacement of the slide apply the multi-block model for a representative seismic motion is applied.

The method was applied successfully to predict the triggering, the motion and the final configuration of the well-documented Higashi Takezawa earthquake-induced slide.

Acknowledgements

The work was funded partly by the project "Novel methodologies for the assessment of risk of ground displacement" under ESPA 2007-2013 of Greece, under action: Bilateral S & T Cooperation between China and Greece. Graduate student of the Hellenic Open University Kelly Gouma assisted in the analysis of the case study. Graduate students of the Hellenic Open University P. Sidiropoulos and J. Bakratzas assisted in the collection of the laboratory tests.

Author details

Constantine A. Stamatopoulos^{1,2*}

Address all correspondence to: k.stam@saa-geotech.gr

1 Hellenic Open University, Athens, Greece

2 Stamatopoulos and Associates Co, Greece

References

- [1] Deng J., Kameya H., Miyashita Y., J., Kuwano R., Koseki J. Study on dip slope failure at Higashi Takezawa induced by 2004 Niigata-Ken Chuetsu earthquake. *Soils and Foundations* Vol. 51. 2011. No. 5, 929-943. Oct.
- [2] Sun P., Wang F., Yin Y., Wu S.. An experimental study of the mechanism of rapid and long run-out landslides triggered by Wenchuan earthquake. *Seismology and geology*. 2010, Vol. 32., No. 1, Mar.
- [3] Sassa, K., Fukuoka, H., Scarascia-Mugnozza, G., Evans, S. Earthquake-induced landslides: Distribution, motion and mechanisms. Special Issue of *Soils and Foundations*, Japan Geotechnical Society. 1996. 53-64.
- [4] Newmark, N. M. Effect of earthquakes on dams and embankments, *Geotechnique*, Vol. 15, No. 2, London, England. 1965. June, 139-160.
- [5] Ambroseys N. and Menu J. Earthquake induced ground displacements, *Earthquake engineering and structural dynamics*. 1988. 16, 7, 985-1006.
- [6] Stamatopoulos, C. A. Sliding System Predicting Large Permanent Co-Seismic Movements of Slopes. *Earthquake Engineering and Structural Dynamics*. 1996. Vol. 25, No, 10, 1075-1093.

- [7] Deng, J., Tsutsumi, Y, Kameya, H., Koseki, J. A Modified Procedure to Evaluate Earthquake-induced Displacement of Slopes Containing a Weak Layer. *Soils and Foundations*. 2010, 50, 3; 413-420
- [8] Stamatopoulos C. A., Mavromihalis C, Sarma S. Correction for geometry changes during motion of sliding-block seismic displacement, *ASCE, Journal of Geotechnical and Geoenvironmental Engineering*. 2011, 137 (10), 926-938.
- [9] Wang G. and Sassa K. Post-failure mobility of saturated sands in undrained load-controlled ring shear tests. *Can. Geotech J.* 2002, 39(4), 821–837.
- [10] Wang, G., Sassa K. Fukuoka H. and Tada T. Experimental study on the shearing behavior of saturated silty soils based on ring shear tests. *Journal of geotechnical and geoenvironmental engineering*. 2007, 319-333.
- [11] Igwe O., Sassa K., Wang F. The influence of grading on the shear strength of loose sands in stress-controlled ring shear tests. *Landslides*. 2007, 4, 43–51.
- [12] Igwe O., Sassa K., Fukuoka H. The geotechnical properties of sands with varying grading in a stressControlled Ring Shear Tests. *The Electronic Journal of Geotechnical Engineering*. 2009, 14.
- [13] Trandafir, A.C. and Sassa, K. Seismic triggering of catastrophic failures on shear surfaces in saturated cohesionless soils. *Canadian Geotechnical Journal*. 2005, Vol. 42, No. 1, 229-251.
- [14] Okada Y., Sassa K., Fukuoka H. Excess pore pressure and grain crushing of sands by means of undrained and naturally drained ring-shear tests, *Engineering Geology* 75, 2004, 325–343
- [15] Sassa K., Wang F. *Progress in Landslide science*. Department of prevention research of Kyoto. Chapters 6, 7. 2007, 90-106.
- [16] Gerolymos N. and Gazetas G. A model for grain-crushing-induced landslides - Application to Nikawa, Kobe 1995, *Soil Dynamics and Earthquake Engineering* 27. 2007, 803-817.
- [17] Stamatopoulos C., Korai C. Constitutive and multi-block modeling of slides on saturated sands along slip surfaces. 7th Hellenic conference of Geotechnical engineering, Athens, Greece. 2014 (in press)
- [18] Sassa K., Fukuoka H.. Excess pore pressure and grain crushing of sands by means of undrained and naturally drained ring-shear tests. *Engineering Geology*. 2004. pp. 325-343
- [19] Sadrekarimi, A. and Olson S. M. Shear Band Formation Observed in Ring Shear Tests on Sandy Soils. *Journal of Geotechnical and Geoenvironmental Engineering, ASCE*. 2010, Vol. 136, No. 2. 366-375.

- [20] Sarma S.K. Stability analysis of embankments and slopes. *Journal of Geotechnical Engineering ASCE*. 1979, Vol.105, No. 12, 1511-1524.
- [21] Sarma S.K. and Chlimitzas G. Co-seismic & post-seismic displacements of slopes, 15th ICSMGE TC4 Satellite Conference on "Lessons Learned from Recent Strong Earthquakes". 2001, 25 August, Istanbul, Turkey
- [22] Sarma S. K., Tan D. Determination of critical slip surface in slope analysis, *Geotechnique*, 2006, Vol. 56, 539-550
- [23] Ambraseys N., Srbulov M. Earthquake induced displacements of slopes, *Soil Dynamics and Earthquake Engineering*. 1995, 14, 59-71.

IntechOpen